Mean-Field Molecular Dynamics with Surface Hopping: Application to the Aqueous Solvated Electron†

Kim F. Wong and Peter J. Rossky*

Institute for Theoretical Chemistry, Department of Chemistry and Biochemistry, University of Texas at Austin, Austin, Texas 78712-1167

Received: October 12, 2000; In Final Form: November 17, 2000

To evaluate the suitability of the combined mean-field/surface hopping (MF/SH) algorithm (Prezhdo, O. V.; Rossky, P. J. *J. Chem. Phys.* **1997**, *107*, 825) for the simulation of realistic chemical environments, we have implemented MF/SH for the nonadiabatic molecular dynamics simulation of the aqueous solvated electron. The relaxation dynamics following both electron injection into pure water and photoexcitation from the equilibrium ground-state electron-water system are considered. The validity of a mean-field evolution of the classical variables is monitored via the deviations of the solvent coordinates and momenta between the mean-field molecular dynamics trajectory and a reference adiabatic molecular dynamics trajectory. In agreement with earlier MF/SH simulations on low dimensional model systems, our results show that divergence between momenta occurs rather rapidly. Present results show that mean-field evolution is valid on a 30−70 fs time scale for ground-state excitation and on a 7−10 fs interval for the electron injection environment. Even for the shorter time cases, the times correspond to ∼20 solvent time steps in simulation. Considering that estimated electronic coherence times for excited state dynamics are considerably shorter, the results indicate that the method is a viable one for high dimensional, strongly interacting systems.

1. Introduction

For many molecular processes in the condensed phase, the fundamental events responsible for the observed chemistry are inherently quantum mechanical in nature. A convenient fully quantum dynamical treatment of the many-body problem presently remains elusive and is normally implemented only approximately even for a relatively small number of degrees of freedom. This is not to say that an accurate qualitative understanding of the prolific phenomena in solution photochemistry, interfacial electron transfer in semiconductors, and biological charge transfer, for example, is beyond the capacity of current methodologies, but only that further innovations and refinements are necessary for accessing complex systems and for obtaining quantitative agreement with experiment. The use of mixed quantum-classical (MQC) molecular dynamics (MD) to elucidate the mechanistic pathways underlying a chemical process in condensed media is a common practice nowadays.[1,2] Although many methodologies have been proposed, no individual approach has been shown to be generally applicable for all system environments. Perhaps a more important consideration is the ease with which the algorithm can be implemented and extended for the simulation of large systems.

Mixed quantum-classical molecular dynamics derives its popularity primarily from its simple concepts, straightforward implementation, and ability to offer insight into key chemical behaviors. The basic idea begins with the Born−Oppenheimer separation of the nuclear degrees of freedom from the electronic. Intuitively, we anticipate the more massive nuclei to follow classical molecular dynamics, while the electrons obey the time-dependent Schrödinger equation. This partitioning of the whole system into a quantum subsystem coupled to a classical subsystem greatly reduces the dimensionality of the quantum problem. The idea of coupling classical variables with the expectation value of quantum observables was first considered by Ehrenfest,[3] who showed that the time evolution of average quantum operators adopts the same form as the classical equation of motion. This observation leads directly to the mean-field trajectory method (MFT),[4−6] whereby classical particles respond to the gradient of the expectation value of the energy, taken over the time dependent subsystem wave function. Although the electronic degrees of freedom respond rigorously to the motion of the classical particles, the classical particles evolve on an effective potential corresponding to an average over quantum eigenstates. This classical evolution on an average potential, however, cannot correctly describe systems having sufficiently different adiabatic energy surfaces such that evolution on different surfaces leads to divergent trajectories. The limitations and validity of the mean-field approach are well documented.[7−10] In particular, for short times, the MFT method can be argued to be optimal.[11] However, for longer times MFT has a key flaw. To see this, we envision a nonadiabatic (NA) event as occurring in three stages: an initial stage where the wave function evolves from a pure state, an intermediate stage as the wave function encounters a region of coupling and evolves into a superposition state, and a final stage outside the coupling region where the wave function evolves adiabatically along alternative channels.[12] During the intermediate stage, the wave function is described by a superposition of different states corresponding to evolution associated with the alternative classical trajectories. The wave functions interfere with each other initially, but as the trajectories diverge beyond the coupling region, all coherence is lost and the corresponding wave functions cease to interact—thus leading to propagation as independent channels. It is this critical asymptotic branching behavior that is absent from the MFT method.

† Part of the special issue "William H. Miller Festschrift".

10.1021/jp0037652 CCC: $20.00
Published on Web 01/18/2001

The traditional approach for incorporating NA transitions within MQC MD is via surface hopping.[13] Surface hopping refers to a basis state expansion of the wave function and the accompanying procedure for determining when a *hop* from one basis state to other states occurs. In the original formulation, the hopping probabilities were calculated from the complex-valued coefficients and transitions were limited to localized avoided crossings. The newest fewest-switches variant[14] determines the transition probability flux via the time derivative of the amplitudes and imposes no preconditions on where transitions can happen. Although several flavors of surface hopping[15−26] have been proposed since its introduction, they all share a common architecture of coexisting quantum subsystems represented by a *primary*, an *auxiliary*, and a *reference* wave function. The primary and reference wave functions arise naturally in the surface hopping model, which distinguishes between the generally mixed-state wave function used for calculating the transition probabilities (primary) and the currently occupied basis state from which transitions occur (reference). The auxiliary wave function governs the classical environmental dynamics; i.e., it governs the calculation of the quantum force on this environment and the total energy. Fundamentally, the primary wave function carries information about quantum interference effects that are important for calculating transition probabilities, and the auxiliary wave function reflects the strategy for selecting the *appropriate* classical trajectory for the total system evolution.

In surface hopping, the reference state is chosen stochastically at each time step based on the primary wave function. Tully's MDQT[21] (molecular dynamics with quantum transitions; originally denoted MDET[14] for electronic transitions) method propagates the classical dynamics via a Hellmann−Feynman force derived from the adiabatic reference state. Here, the auxiliary wave function coincides with the reference wave function, generating adiabatic dynamics interrupted by hops. The primary wave function evolves coherently as a superposition state with a time-dependent Hamiltonian determined by the classical trajectory. For the SPSH[27] (stationary phase/surface hopping) algorithm of Webster et al., the force expression is based on the Pechukas semiclassical evaluation of the electronic-nuclear path integral representation of the propagator.[28] Because the effective nuclear potential is nonlocal in time, this method actually has two auxiliary wave functions—one associated with the beginning of the time step by propagating forward in time the initial reference state and the other associated with the end of the time step by propagating backward in time the final adiabatic reference state. The primary wave function corresponds to the superposition state obtained by time propagation of the reference state at the beginning of every time step. Unlike MDQT, which performs the full evolution coherently, SPSH periodically resets the primary state to a final reference state that contains the largest projection of the primary wave function. Due to the destruction of coherence at the end of each such period, transition probabilities and hence also the dynamics are dependent on this coherence time.[29]

The mean-field with surface hopping approach implemented in the present study of the solvated electron has been introduced earlier.[12] It combines the desirable features of the MFT method and surface hopping into a NA dynamics algorithm. The basic idea is to perform mean-field evolution of the classical particles and to correct the trajectories when the mean-field approximation is no longer valid according to quantitative criteria.[12] NA transitions are affected via the surface hopping prescription where the primary wave function evolves coherently for the entire MD simulation. The validity of the mean-field approach is summarized by the general requirement that trajectories corresponding to evolution on different quantum states do not diverge appreciably from each other.[9] Quantitatively, this condition is expressed in terms of a momentum and coordinate criteria between all pairs of trajectories associated with evolution on different quantum states. Since surface hopping keeps track of the reference state and the reference state typically contributes the most to the mean-field force, the validity criteria are conveniently evaluated by monitoring only the mean-field and reference trajectories. As long as the classical momenta and coordinates from the two trajectories do not diverge, the classical MFT evolution proceeds. If either criterion fails, the auxiliary wave function is projected onto the current reference state, and the evolution restarts from this point. In the case of a surface hop, the currently occupied state switches to a new reference state, and the auxiliary wave function restarts from this new reference state.

From simulations of model two level systems that were specifically designed to mimic the coupling regions and asymptotic limits routinely encountered in condensed phase simulations,[14] one can observe several appealing attributes of MF/SH as compared to both MDQT and SPSH.[12] At high energies, the MDQT, MF/SH, and exact quantum results are in reasonable agreement. At lower energies, when the classical coordinate spends significant amounts of time in the coupling region, MF/SH provides a modest improvement over MDQT in describing the interference effects. The results from the SPSH implementation are effectively identical to MDQT. Further, both MDQT and SPSH preferentially evaluate the NA molecular dynamics within the chosen basis representation. For systems whose *natural* basis representation (i.e., that which most closely mimics the correct eigenstates) differs from the propagation basis chosen, MF/SH was found to be considerably more accurate than either MDQT or SPSH.[12] This feature recommends MF/SH in cases where the preferred basis is not completely clear.

SPSH simulations of solvated electrons[30−32] and halide electron photodetachment,[35] nonetheless, give results that are in reasonable agreement with experiments. Due to the algorithmic complexity and computational requirements associated with the iterative evaluation of the Pechukas expression for the quantum force,[28] the method has not seen much acceptance as a general approach to quantum dynamics in condensed matter. MDQT, on the other hand, is easily implemented and computationally efficient; it has been used to study model proton transfer in solution,[21,36−38] excess electrons in simple liquids,[39,40] internal conversion,[15,41−43] and electron transfer.[44−46] MF/SH shares many of the conveniences of the MDQT algorithm with only about a 2-fold increase in computation cost, associated with the propagation of reference and MF trajectories.

The formalities discussed above notwithstanding, a critical question is the time scale during which the MF propagation remains valid. If this time is too short, then the method will not differ from MDQT. Low dimensional cases were considered in earlier tests.[12] When many degrees of freedom of the classical bath are interacting strongly with the quantum subsystem, it is reasonable to be concerned that the MF and reference state trajectories may diverge, by reasonable quantitative criteria, more rapidly than for the model systems. This concern follows from the fact that *all* coordinates and momenta must remain within the specified tolerances to retain validity. Therefore, a test on a strongly coupled, high dimensional system is needed. The principal criterion for usefulness is that the MF propagation persists for times that are significantly longer than the simulation time step. Correspondingly, one needs to establish that the

behavior of the simulation is not a sensitive function of the criteria for validity of MF propagation. Finally, one wants to establish that MF propagation is valid for times at least as long as the characteristic decoherence time, after which the reduction to an adiabatic state and force is arguably justified.

In the following contribution, we present results from our study of the aqueous solvated electron system using the MF/SH method. Since the environment is treated classically, nuclear tunneling—for example, of the protons in the water—is not addressed.[8,9,14,21] Also, quantum decoherence is not explicitly integrated within the method, except as an aftermath of a MF projection. The current and forthcoming studies focus on both algorithmic development for the simulation of NA processes in condensed media and physical understanding of a realistic prototype exhibiting intimate coupling between the quantum and classical systems. Experimentally accessible, the solvated electron[47−57] represents one of the simplest models which partitions in an obvious manner into a quantum subsystem coupled to a classical solvent environment. Bound states arise for electrons in polar solvents due to self-trapping in a solvent cage. Fluctuations in the solvent molecules modulate the states of the system and completely determine the quantum evolution. Correspondingly, the state of the electron influences the particular realization of the solvent classical trajectories, much as an atomic ion. This dynamic interplay between the quantum and classical systems makes the solvated electron an ideal candidate for exploring the features of MF/SH.

The structure of this paper is as follows: After briefly reviewing the mixed quantum-classical formalism and surface hopping, we outline the details of the MF/SH algorithm. Results from the MF/SH treatment of the solvated electron will be presented in section 3. We conclude in section 4 with a discussion of promising features and potential improvements to the technique and provide some comments regarding future developments of this MQC MD method.

2. Theory and Algorithm Development

Mean-field with surface hopping synthesizes several practical methods into a unified nonadiabatic molecular dynamics procedure. In subsection 2.1, we present the classical trajectory[58] formalism that is at the heart of many MQC methods. MF/SH is discussed in subsection 2.2 and the actual implementation, with explicit reference to the solvated electron system, is outlined in subsection 2.3.

2.1. Mixed Quantum−Classical Molecular Dynamics. Central to mixed quantum−classical molecular dynamics is the assumption that classical particles pursue trajectories and that a corresponding wave function, deriving its time dependence solely from a parametric dependence on the classical coordinates, completely specifies the state of the coupled quantum system. Although formally presumed to exist, in practice the trajectories are built up, self-consistent with the wave function evolution, from a sequence of time-ordered configurations. One direct approach to obtaining the equation of motion for the classical particles begins by writing the total energy of the quantum−classical system as

$$E^{\mathrm{tot}} = \left[\frac{M\dot{\mathbf{R}}(t)^2}{2} + V^{\mathrm{cl}}(\mathbf{R}(t))\right] + \langle\Psi(\mathbf{r};\mathbf{R}(t))|H^{\mathrm{q}}(\mathbf{r};\mathbf{R}(t))|\Psi(\mathbf{r};\mathbf{R}(t))\rangle = E^{\mathrm{cl}} + E^{\mathrm{q}} \quad (1)$$

where the terms in square brackets denote respectively the classical kinetic and potential energy and the final term, the expectation value of the quantum energy, as an explicit function of the set of quantum coordinates **r** and an implicit function of the set of classical coordinates **R**. For notational simplicity, the classical particles here are assumed to have equal mass *M*, and the angled brackets correspond to the usual Dirac notation for integration with respect to the quantum variables. Note that the time dependence of the wave function and the Hamiltonian arises purely from the parametric dependence on the classical variables. Differentiating with respect to time and observing the conservation of energy, we obtain Newton's equation of motion

$$M\ddot{\mathbf{R}} = \mathbf{F}^{\mathrm{cl}} + \mathbf{F}^{\mathrm{q}} \quad (2)$$

where

$$\mathbf{F}^{\mathrm{cl}} = -\nabla_{\mathbf{R}} V^{\mathrm{cl}}(\mathbf{R}) \quad (3)$$

describes the contribution to the force from the classical−classical interactions and

$$\mathbf{F}^{\mathrm{q}} = -\nabla_{\mathbf{R}}\langle\Psi(\mathbf{r};\mathbf{R})|H^{\mathrm{q}}(\mathbf{r};\mathbf{R})|\Psi(\mathbf{r};\mathbf{R})\rangle \quad (4)$$

defines the quantum force on the classical particles due to interaction with the quantum subsystem. For the special case in which Ψ is an eigenstate of the Hamiltonian, the quantum force term reduces to the Hellmann−Feynman force[59]

$$\mathbf{F}^{\mathrm{q}} = -\langle\Psi(\mathbf{r};\mathbf{R})|\nabla_{\mathbf{R}} H^{\mathrm{q}}(\mathbf{r};\mathbf{R})|\Psi(\mathbf{r};\mathbf{R})\rangle \quad (5)$$

Simultaneously, the wave function describing the quantum subsystem evolves according to Schrödinger's equation

$$i\hbar\frac{\partial\Psi(\mathbf{r},t;\mathbf{R})}{\partial t} = H^{\mathrm{q}}(\mathbf{r};\mathbf{R})\Psi(\mathbf{r},t;\mathbf{R}) \quad (6)$$

as a consequence of the time-dependent Hamiltonian, $H^{\mathrm{q}}(\mathbf{r};\mathbf{R}(t))$, that changes in response to the classical trajectory. From a basis state expansion of the wave function,

$$\Psi(\mathbf{r},t;\mathbf{R}) = \sum_j c_j(t)\phi_j(\mathbf{r};\mathbf{R}(t)) \quad (7)$$

we obtain the equation of motion for the amplitudes as

$$i\hbar\dot{c}_{\mathrm{k}} = \sum_j c_j(V_{kj} - i\hbar\mathbf{d}_{kj}\cdot\dot{\mathbf{R}}) \quad (8)$$

where $V_{kj} = \langle\phi_k(\mathbf{r};\mathbf{R})|H^{\mathrm{q}}(\mathbf{r};\mathbf{R})|\phi_j(\mathbf{r};\mathbf{R})\rangle$ reduces to the electronic energy ϵ_j for the case of an adiabatic basis set and $\mathbf{d}_{kj} = \langle\phi_k(\mathbf{r};\mathbf{R})|\nabla_{\mathbf{R}}|\phi_j(\mathbf{r};\mathbf{R})\rangle$ defines the NA coupling between states ϕ_k and ϕ_j due to breakdown of the Born−Oppenheimer approximation. Equations 2 and 8 describe the dynamics of a coupled quantum−classical system. The various MQC MD methods differ in their interpretation and choice of the quantum force that will give the correct evolution of the total system.

2.2. Mean-Field with Surface Hopping Algorithm. In the MF/SH algorithm,[12] the classical variables evolve according to eq 2 where the auxiliary wave function Ψ entering in the quantum force expression (eq 4) is a superposition state. Application of the mean-field approach for a two-state quantum subsystem coupled to a single classical coordinate is valid only when

$$|(P_2 - P_1)/(P_2 + P_1)| \ll 1 \quad (9)$$

$$|(R_2 - R_1)|/a_0 \ll 1 \quad (10)$$

where a_0 is an arbitrary quantum length scale which we have chosen in this context to be equal to the Bohr radius, and P_1, P_2, R_1, and R_2 are classical momenta and coordinates from trajectories propagated on two different potential energy surfaces.[9] A generalization of the criteria from a two state-single particle system to a many state-many coordinate system is[12]

$$\frac{|\mathbf{P}^{\alpha}_{[MT]} - \mathbf{P}^{\alpha}_{[RT]}|}{|\mathbf{P}^{\alpha}_{[MT]} + \mathbf{P}^{\alpha}_{[RT]}|} \equiv \Lambda_{\mathbf{P}} < \lambda_{\mathbf{P}}, \text{ all } \alpha \tag{11}$$

$$|\mathbf{R}^{\alpha}_{[MT]} - \mathbf{R}^{\alpha}_{[RT]}| \equiv \Lambda_{\mathbf{R}} < \lambda_{\mathbf{R}}, \text{ all } \alpha \tag{12}$$

where the subscripts [MT] and [RT] denote respectively the mean-field and reference trajectories, the index α runs over all classical particles, and $\lambda_{\mathbf{P}}$ and $\lambda_{\mathbf{R}}$ are choices of physically plausible momentum and coordinate criteria. Within a trajectory scheme, the mean-field momenta and positions are obtained via mean-field molecular dynamics, while the reference quantities are obtain by adiabatic molecular dynamics. Because the surface hopping reference state typically carries the largest contribution in the auxiliary wave function, monitoring the deviations between MF and reference trajectories, rather than between all pairs of trajectories, should estimate the mean-field validity efficiently and with the same physical content. The momentum criterion reflects, for example, the breakdown of the mean-field approximation near turning points where classical evolutions corresponding to different quantum states can evolve in opposite directions. The position criterion accounts for the failure of the mean-field approach to give correct asymptotic behavior of trajectories outside regions of NA coupling. In instances where either of the two criteria fail for any classical particle α, the auxiliary wave function corresponding to the mean-field trajectory is projected onto the currently occupied state and the simulation restarts using this reference wave function for the current MF nuclear configuration. NA transitions are incorporated in the method via the fewest-switches surface hopping (FSSH) prescription.

In the current implementation, the values of $\lambda_{\mathbf{P}}$ and $\lambda_{\mathbf{R}}$ enter as adjustable parameters. A stringent set of criteria (small values of $\lambda_{\mathbf{P}}$ and $\lambda_{\mathbf{R}}$) give mean-field dynamics interrupted by frequent projections of the superposition state unto a pure state. As already noted, in the most stringent criteria limit, MF/SH reduces to MDQT. A more flexible set of criteria permits the system to evolve for longer times under the mean-field force before a projection. A reasonable, physically sensible value for $\lambda_{\mathbf{P}}$, for example, is $\sim 0.10-0.20$.

An artifact of MF/SH is that the reference trajectory is piecewise continuous interrupted by resets to the current MF nuclear configuration following a MF projection or a surface hop. This feature, however, has no important consequence if these discontinuities are small, as expected. This will be demonstrated for the present example. After a mean-field projection, the solvent velocities must be adjusted in order to maintain energy conservation. Although these adjustments are small (~ 0.05 eV), the question that remains is how should the adjustment be performed. In the case of surface hopping, using the direction of the NA coupling between the currently occupied state ϕ_k and the new state ϕ_j is well justified.[14] Here, we choose to adjust the solvent velocities in the direction of an effective NA coupling defined as a sum of NA couplings between the occupied state and all other states weighted by the populations $|c_j|^2$:

$$\tilde{\mathbf{d}}_{eff}{}^{\alpha} \equiv -\sum_j |c_j|^2 \mathbf{d}^{\alpha}{}_{kj} = \sum_j |c_j|^2 \mathbf{d}^{\alpha}{}_{jk}* \tag{13}$$

Redistribution of the small energy changes among the many nuclear degrees of freedom should not significantly perturb the dynamics of the whole system.

2.3. Steps in MF/SH Implementation for the Hydrated Electron. The simulated system is identical to the electron−water model implemented in earlier work.[27] It is described by a cubic cell of side length 18.17 Å containing 200 classical flexible SPC water molecules[66,67] and one quantum mechanical electron with a total solvent density of 0.997 g/cm^3 at an initial temperature of 300 K. Standard periodic boundary conditions are employed and all interactions are evaluated with a smooth spherical cutoff terminating at 8.0 Å.[68] The electron−water interactions are described by a previously developed pseudopotential.[69] Utilizing the block Lanczos[70] algorithm with a spectral filter preconditioning scheme, the lowest 16 adiabatic eigenstates of the excess electron are evaluated on a 16^3 grid in a plane-wave representation.[27] NA MQC MD is performed by using the MF/SH procedure, and the classical equation of motion is integrated with the velocity Verlet algorithm using a 0.50 fs MD time step. Propagation of the expansion coefficients is done using the fourth-order Runge−Kutta numerical integration method.[71]

Two types of experimental conditions are modeled in the current study. For the simulation of electron photoinjection into water, the initial solvent configuration corresponds to an equilibrated pure water configuration obtained from a long classical MD trajectory.[27,72] One of the relatively high energy adiabatic excited states ϕ_k (in the range 1.9−2.2 eV above the vacuum level) is selected as the initial primary, auxiliary, and reference wave functions. We have examined 15 trajectory examples in this work. For simulation of the pump−probe experiment,[30] the starting solvent configuration corresponds to an equilibrated ground state electron−water system obtained by first adding an excess electron into neat water and equilibrating the resulting ground-state electron for 15 ps. Following equilibration, we ran a 35 ps adiabatic ground-state trajectory and randomly select 20 configurations from this trajectory as starting points. The electron is then promoted from the ground state to the first excited state, and the simulation begins with the primary, auxiliary, and reference wave functions set equal to this excited state.

The momentum and coordinate mean-field criteria enter in the method as parameters. To explore the effects of the choice of mean-field conditions, we execute several trajectories from the same solvent configuration with different criteria. Because the solvent configuration number is used as the initial seed for the random number generator, the trajectories within each MD set (started form the same solvent configuration) share a common random number sequence. For all trajectories, we set the coordinate criterion $\lambda_{\mathbf{R}}$ equal to the Bohr radius, while we set the momentum criterion $\lambda_{\mathbf{P}}$ either to 0.05, 0.10, 0.20, or 0.50. In agreement with earlier findings from simulations of model systems,[12] we observe the violation of the momentum criterion long before that of the coordinate criterion. Hence, for the solvated electron system, we can discard the position criterion altogether and only monitor the deviations in the solvent molecule momenta between the mean-field and reference trajectories. As noted earlier, one would expect $\lambda_{\mathbf{P}}$ values of

~0.1−0.2 to be plausible practical choices, and 0.05 and 0.50 are considered likely extremes.

These choices are related, after all, to some characteristic length and velocity scales. For the simpler one-dimensional model, the momentum criterion can be written as

$$|(P_2 - P_1)/(P_2 + P_1)| = \lambda_{\mathbf{p}} \tag{14}$$

where we have replaced the inequality with an equality so that we can isolate the very instance of a MF violation. Let us also express the momentum of the particle on the first surface in terms of the momentum on the second surface, $P_1 = \beta P_2$, where β is a scale factor. Solving for this scale factor, we obtain

$$\beta = \begin{cases} (1 - \lambda_{\mathbf{p}})/(1 + \lambda_{\mathbf{p}}) & P_1 \text{ and } P_2 \text{ in the same direction} \\ -(1 - \lambda_{\mathbf{p}})/(1 + \lambda_{\mathbf{p}}) & P_1 \text{ and } P_2 \text{ in opposite directions} \end{cases} \tag{15}$$

For $\lambda_{\mathbf{p}} = 0.10 - 0.20$, the momentum on the first surface is 82−67% ($\beta = 0.82-0.67$) of the momentum on the second surface. A criterion of 0.05 and 0.50 scales the momentum by 0.90 and 0.33, respectively. Although more intricate to analyze, the plausible choice of $\lambda_{\mathbf{p}} = 0.10-0.20$ for the multidimensional case should carry the same physical content as for the one-dimensional model.

Under these criteria, MF/SH distinguishes distinct evolutions when the particles are separated by a characteristic length scale of approximately the Bohr radius (eq 10) and a velocity scale of ~0.18−0.33. A length scale of the Bohr radius is an appropriately stringent criterion, because the divergence in the coordinate is less than a chemical bond. When the asymptotic products associated with evolution on distinct surfaces are spatially separated by only ~0.5 Å, one does not have sufficient resolution to discriminate that the asymptotic channels are not identical. Mean-field propagation under this condition, therefore, is practical. As an offspring of the WKB approximation, MFT breaks down near classical turning points, where classical evolutions corresponding to different quantum states can proceed in opposite directions. We have verified from direct simulation data that, for $\lambda_{\mathbf{p}} = 0.10 - 0.20$, classical evolution in opposite directions persists for only a single MD time step (0.50 fs) and that this is the very time step that triggers the MF violation. Out of all violations accumulated along a MF/SH trajectory, less than 10% are due to momenta proceeding in opposite directions. Although it is seductively appealing to be able to assign a priori these quantitative criteria based solely on intuitive insight of the system under consideration, it is not possible for the momentum criterion. To do so would require knowledge of the ground and excited state topological details—an endeavor that is practically impossible. However, one only needs to run a few sample trajectories for the system under study to determine if a set of criteria is appropriate. As long as the classical momenta on different surfaces do not proceed in opposite directions for more than a few time steps, MF/SH should be viable.

We now outline the algorithm for the simulation of the excess electron in water system. Classical coordinates $\mathbf{R}(t)$, half-step velocities $\dot{\mathbf{R}}$ $(t - \Delta t/2)$, velocities $\dot{\mathbf{R}}$ $(t - \Delta t)$, and the quantum state corresponding to the desired initial conditions are specified. Although MF/SH in general can accommodate a diabatic representation, we choose an adiabatic representation of the wave function in the present study. The system starts in a pure state with the expansion coefficients initialized as $c_k = 1.0$ and all others set to zero. The primary, auxiliary, and reference wave functions are identical at time $t = 0$. Two adiabatic MD time steps are taken in the beginning to obtain NA coupling/velocity dot products needed for the interpolation/extrapolation procedure discussed below. Initially, the reference ([RT]) nuclear coordinates and velocities coincide with the corresponding mean-field ([MT]) values.

For Every MD Time Sequence, t_m, Perform the Following: *Mean-Field Trajectory. Step 1. Eigenvalue Problem.* For the current nuclear configuration $\mathbf{R}_{[\mathrm{MT}]}(t_m)$, compute the set of adiabatic eigenstates $\{\phi_{[\mathrm{MT}]}(t_m)\}$.

Step 2. Classical Dynamics. Compute the mean-field forces corresponding to the propagated superposition state and compute the classical solvent forces. Integrate the velocities to the current time step

$$\dot{\mathbf{R}}_{[\mathrm{MT}]}(t_m) = \dot{\mathbf{R}}_{[\mathrm{MT}]}(t_m - \Delta t/2) + \frac{1}{2}\Delta t(\mathbf{F}^{\mathrm{q}}_{[\mathrm{MT}]}(t_m) + \mathbf{F}^{\mathrm{cl}}_{[\mathrm{MT}]}(t_m))/\mathrm{M} \tag{16}$$

Step 3. NA Coupling/Velocity Dot Products. From the sets of eigenstates $\{\phi_{[\mathrm{MT}]}(t_m)\}$ and $\{\phi_{[\mathrm{MT}]}(t_m - \Delta t)\}$, compute the set of approximate NA coupling/velocity dot products using the differentiation chain rule

$$[\mathbf{d}_{kl} \cdot \dot{\mathbf{R}}](t_m - \Delta t/2) \approx \frac{1}{2\Delta t}(\langle\phi_k(t_m - \Delta t)|\phi_l(t_m)\rangle - \langle\phi_k(t_m)|\phi_l(t_m - \Delta t)\rangle) \tag{17}$$

Step 4. Wave Function Propagation. With a smaller *quantum* time step $\delta t = 0.001\Delta t$, propagate the expansion coefficients (eq 8) corresponding to the primary and auxiliary wave functions from $t_m - \Delta t$ to t_m using the fourth-order Runge−Kutta numerical integration method. We linearly interpolate between $\epsilon_k(t_m - \Delta t)$ and $\epsilon_k(t_m)$ to obtain the intermediate $\epsilon_k = V_{kk}$ values needed for the integration. Likewise, we interpolate and extrapolate from $[\mathbf{d}_{kl} \cdot \dot{\mathbf{R}}](t_m - 3\Delta t/2)$ to $[\mathbf{d}_{kl} \cdot \dot{\mathbf{R}}](t_m - \Delta t/2)$ in order to obtain NA coupling/velocity dot products between $t_m - \Delta t$ and t_m. Simultaneous with the wave function propagation, the FSSH probabilities,

$$g_{kj}(t_m) = \frac{\int_{t_m - \Delta t}^{t_m} \mathrm{d}t\, b_{jk}(t_m - \Delta t)}{|c_k(t_m)|^2} \tag{18}$$

where

$$b_{kl} = 2\hbar^{-1}\,\mathrm{Im}(c_k^* c_l V_{kl}) - 2\,\mathrm{Re}(c_k^* c_l \mathrm{d}_{kl} \cdot \dot{\mathbf{R}}) \tag{19}$$

are numerically integrated from $t_m - \Delta t$ to t_m for all states j using the Runge−Kutta integration time step δt.

Step 5. Surface Hopping. Generate a random number ξ uniformly distributed on the interval (0,1) and compare it with the transition probabilities calculated in the previous step. A switch to state $j = n + 1$ occurs if $\sum_{j=1}^{n} g_{kj} < \xi < \sum_{j=1}^{n+1} g_{kj}$, for $0 < n < K$, where K is the total number of trajectories.

Reference Trajectory. Step A. Eigenvalue Problem. For the current solvent nuclear configuration $\mathbf{R}_{[\mathrm{RT}]}(t_m)$, compute the set of adiabatic eigenstates $\{\phi_{[\mathrm{RT}]}(t_m)\}$.

Step B. Classical Dynamics. Compute the Hellmann−Feynman forces corresponding to the reference state k and compute the classical solvent forces. Integrate the velocities to the current time step:

$$\dot{\mathbf{R}}_{[\mathrm{RT}]}(t_m) = \dot{\mathbf{R}}_{[\mathrm{RT}]}(t_m - \Delta t/2) + \frac{1}{2}\Delta t(\mathbf{F}^{q}_{[RT]}(t_m) + \mathbf{F}^{\mathrm{cl}}_{[\mathrm{RT}]}(t_m))/M \tag{20}$$

Step 6. Mean-Field Criteria Check. If a hop did not occur, check the mean-field validity criteria:

$$\frac{|\mathbf{P}^{\alpha}_{[MT]} - \mathbf{P}^{\alpha}_{[RT]}|}{|\mathbf{P}^{\alpha}_{[MT]} + \mathbf{P}^{\alpha}_{[RT]}|} \equiv \Lambda_{\mathbf{P}} \overset{?}{<} \lambda_{\mathbf{P}} \quad \text{for all } \alpha \tag{21}$$

$$\frac{|\mathbf{R}^{\alpha}_{[MT]} - \mathbf{R}^{\alpha}_{[RT]}|}{|\mathbf{R}^{\alpha}_{[MT]} + \mathbf{R}^{\alpha}_{[RT]}|} \equiv \Lambda_{\mathbf{R}} \overset{?}{<} \lambda_{\mathbf{R}} \quad \text{for all } \alpha \tag{22}$$

If $\Lambda_{\mathbf{P}} > \lambda_{\mathbf{P}}$ or $\Lambda_{\mathbf{R}} > \lambda_{\mathbf{R}}$, the auxiliary wave function is projected onto the currently occupied state by setting $c_l^{prim} = c_l^{aux} = \delta_{kl}$, where k denotes the reference state.

Step 7. Velocity Adjustment. After a NA transition, the classical nuclear velocities are adjusted in the direction of the NA coupling vector to absorb/release the quantum energy gap accompanying a relaxation/excitation process.[21] For the case of a mean-field projection, the nuclear velocities are adjusted in the direction of an effective NA coupling defined as a sum of NA couplings between the occupied state k and all other states j weighted by the populations (eq 13).

Step 8. Update Nuclear Coordinates and Velocities. Integrate the nuclear coordinates and half-step velocities by one MD time step:

$$\mathbf{R}_{[MT]}(t_m + \Delta t) = \mathbf{R}_{[MT]}(t_m) + \Delta t\dot{\mathbf{R}}_{[MT]}(t_m) + \frac{1}{2}\Delta t^2(\mathbf{F}^{q}_{[MT]}(t_m) + \mathbf{F}^{cl}_{[MT]}(t_m))/M \tag{23}$$

$$\mathbf{R}_{[RT]}(t_m + \Delta t) = \mathbf{R}_{[RT]}(t_m) + \Delta t\dot{\mathbf{R}}_{[RT]}(t_m) + \frac{1}{2}\Delta t^2(\mathbf{F}^{q}_{[RT]}(t_m) + \mathbf{F}^{cl}_{[RT]}(t_m))/M \tag{24}$$

$$\dot{\mathbf{R}}_{[MT]}\left(t_m + \frac{1}{2}\Delta t\right) = \dot{\mathbf{R}}_{[MT]}(t_m) + \frac{1}{2}\Delta t(\mathbf{F}^{q}_{[MT]}(t_m) + \mathbf{F}^{cl}_{[MT]}(t_m))/M \tag{25}$$

$$\dot{\mathbf{R}}_{[RT]}\left(t_m + \frac{1}{2}\Delta t\right) = \dot{\mathbf{R}}_{[RT]}(t_m) + \frac{1}{2}\Delta t(\mathbf{F}^{q}_{[RT]}(t_m) + \mathbf{F}^{cl}_{[RT]}(t_m))/M \tag{26}$$

Step 9. Reinitialization of Reference Dynamics. After a surface hop or a mean-field projection, the reference dynamical quantities are reinitialized to the mean-field dynamical quantities. The reference trajectory data are replaced by the corresponding mean-field positions $\mathbf{R}_{[MT]}(t_m + \Delta t) \rightarrow \mathbf{R}_{[RT]}(t_m + \Delta t)$, velocities $\dot{\mathbf{R}}_{[RT]}(t_m) \rightarrow \dot{\mathbf{R}}_{[RT]}(t_m)$, and half-velocities $\dot{\mathbf{R}}_{[MT]}(t_m + {}^1/_2\Delta t) \rightarrow \dot{\mathbf{R}}_{[RT]}(t_m + {}^1/_2\Delta t)$.

3. Results for the Aqueous Solvated Electron

In this section, we present the results from our simulations of the electron photoexcitation and electron injection experiments. The trajectories are analyzed with respect to the choice of mean-field momentum criterion, and comparisons with former SPSH simulations are made when appropriate.

We first consider the behavior of the solvated electron following photoexcitation from the equilibrated ground state to the first excited state. Figure 1a−d presents a dynamical history of the adiabatic eigenstates for representative trajectories initiated from the same equilibrium ground state solvent configuration with momentum criterion set equal to 0.05, 0.10, 0.20, and 0.50, respectively. The bold trace shows the currently occupied reference state, while the vertical tick marks along the horizontal line at −4.5 eV indicate the time associated with a mean-field validity failure. The energy conservation for the whole system is also monitored via the horizontal line fluctuating about 0 eV.

At time $t = 0$, the equilibrium ground state electron is promoted to the first excited state. As the solvent molecules rearrange to accommodate the charge density of the newly occupied state, the energies of the ground state and low lying excited states increase dramatically, resulting in a sizable energy gap between the first excited state and higher lying states. The energy of the first excited-state fluctuates about a constant value for about 200−600 fs, after which the electron undergoes a nonradiative transition back to the ground state. As observed previously,[32] the solvent relaxation following photoexcitation typically acts to raise the energy level of the ground state to within 0.5 eV of the first excited state until radiationless decay drops the electron back to the ground state. Subsequent equilibration in the ground-state reforms the energy gap between the equilibrium solvated electron and the band consisting of the first three excited states.

Although qualitatively similar to the SPSH simulations of the photoexcited solvated electron, these MF/SH trajectories do exhibit features that are unique to the current method. Immediately noticeable are the differences in the trajectories as a consequence of the choice of MF momentum criterion. From the time of the initial formation of the first excited state to about 190 fs, the paths through state space for all four simulations appear to be identical despite the fact that the simulation with MF criterion set equal to 0.05 has experienced eight MF projections, while the one with criterion equal to 0.50 has failed only once. The NA transition at 192 fs following photoexcitation causes the $\lambda_{\mathbf{P}} = 0.05$ trajectory to diverge from the other three systems. The $\lambda_{\mathbf{P}} = 0.10$, 0.20, and 0.50 trajectories resemble each other for about 350 fs, after which the $\lambda_{\mathbf{P}} = 0.10$ system undergoes relaxation to the ground state (360 fs) and evolves differently from the latter two systems. This divergence of the paths shown in Figure 1 appears to be a direct result of the stochastic element in the fewest-switches surface hopping method. Following a NA transition, the ground state force will be dramatically different from the excited-state force driving the unrelaxed systems. Trajectory differences after these transitions therefore are to be expected. These differences change the solvent dynamics, which in turn alter the quantum subsystem evolution. On the other hand, Figure 1c,d shows two state space trajectories diverging from each other after 350 fs, although both systems continue to evolve from an excited-state force for another 200 fs. The $\lambda_{\mathbf{P}} = 0.20$ system experiences a MF projection at 355 fs for a total of five projections, while the $\lambda_{\mathbf{P}} = 0.50$ system has undergone three projections and continues to evolve from a MF force until a validity violation at 375 fs. For these two trajectories, the divergence is due to quantum forces resulting from the different time development of the superposition auxiliary wave function in the MF/SH algorithm with different criteria.

The close resemblance among parts b and d of Figure 1 at early times should not be interpreted as suggesting that the MF projections are unimportant for short time dynamics. It is apparent that at long times the state space trajectories are distinct; however, examination of the solvent trajectories indicates that this is the aftermath of small accumulated variations in the nuclear paths at early times. Furthermore, these variations alter the evolution of the density matrix elements as manifest in the various NA transition times. Recall that we initiate the photoexcitation simulations with the same initial conditions and with the same random number seed; each time

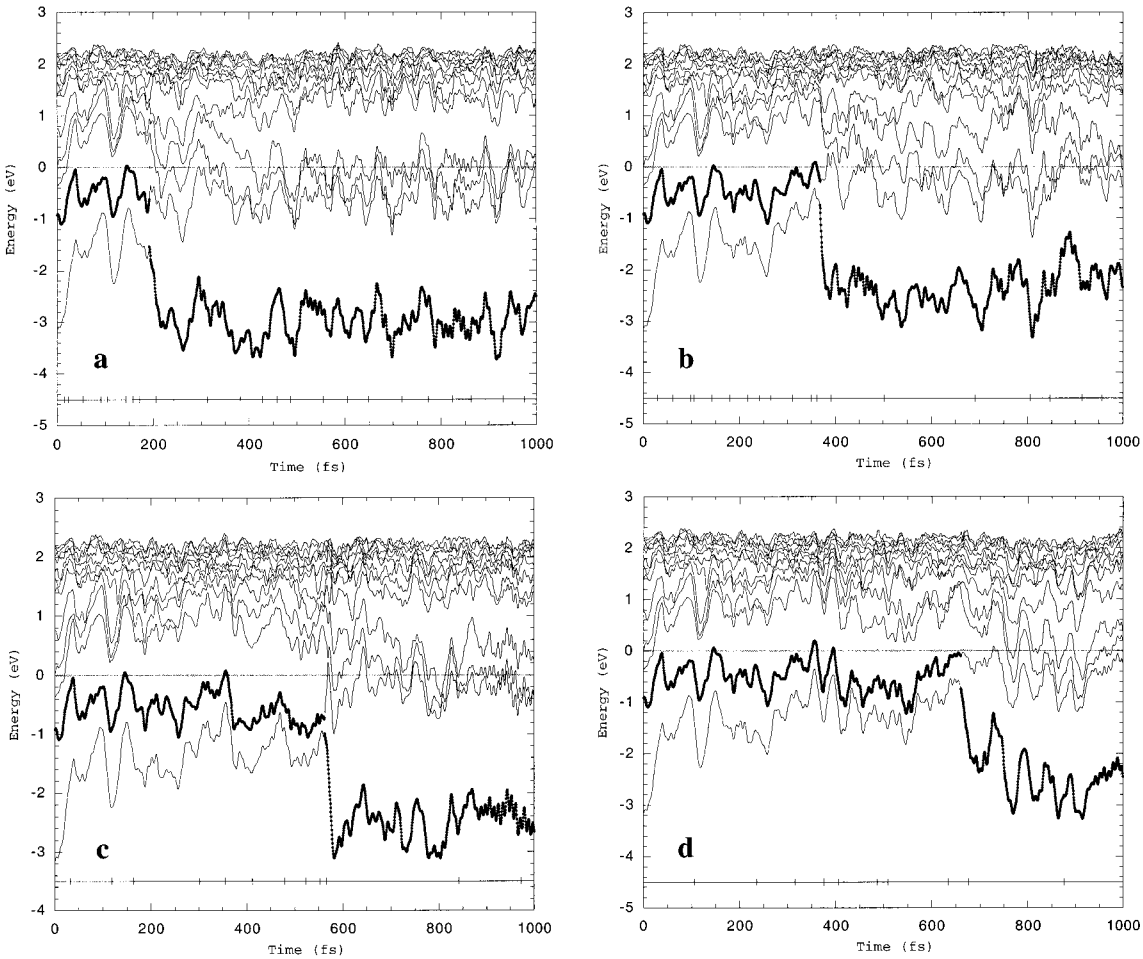

Figure 1. Dynamical history of the adiabatic eigenstates for a typical set of trajectories describing electron photoexcitation with mean-field momentum criterion $\lambda_{\mathbf{P}}$ set equal to (a) 0.05, (b) 0.10, (c) 0.20, and (d) 0.50. Initial conditions and random number sequences are identical in all four cases. The bold trace shows the currently occupied state, while the vertical ticks along the horizontal line at −4.5 eV indicate the times associated with a mean-field validity failure. The fluctuating line at 0 eV indicates deviations from energy conservation.

step in Figure 1a−d has associated with it the same random number. These identical random numbers are compared with each set of transition probabilities g_{kj} for the various $\lambda_{\mathbf{P}}$ simulations. The observed variations in transition times are due to variations in the g_{kj} as the nuclear paths diverge. Figure 1 does not delineate a particular projection (such as the one at 355 fs for the $\lambda_{\mathbf{P}} = 0.20$ system) as dynamically more important than others. Based on the observations made above, and similar observations for other representative trajectories (not shown), we find that the moderate criteria $\lambda_{\mathbf{P}} \sim 0.10-0.20$ lead to well-behaved trajectories. The MF criteria persist for an excited-state reference system for an average of 30−70 fs. For $\lambda_{\mathbf{P}} = 0.20$, this corresponds to 70 classical molecular dynamics steps and about 25 times the coherence time between the ground and excited state.[33,34] Further, the dynamics observed is evidently not a sensitive function of the choice of $\lambda_{\mathbf{P}}$. Hence, for this case, the MF/SH algorithm is clearly completely viable.

Next, we examine the results from our simulation of the electron injection experiment. Figures 2 and 3 show representative paths through state space with the momentum criterion $\lambda_{\mathbf{P}}$ again set equal to 0.05, 0.10, 0.20, and 0.50. At time $t = 0$, an energetic electron is placed inside a volume of neat water. The quantum solute quickly cascades through the closely spaced periodic "continuum" states into the lower three p-like excited states and finally into the ground state. We observe a systematic lowering of the occupied energy level as well as levels below the occupied state during the relaxation. Decay to the ground state is accompanied by the normal precipitous drop in the ground-state energy level and separation of the three lowest excited state states from the continuum band by about a 1.0 eV gap. These features are the typical behavior observed in the original SPSH simulation of the solvated electron.[67,72]

In contrast to the results presented just above, the quantum dynamics here responds more sensitively to the choice of momentum criterion. Most apparent is the difference in the elapsed time after which state space trajectories associated with different mean-field criteria deviate from each other. Under the ground state photoexcitation condition, the four choices of criterion give trajectories that closely resemble each other up to about 190 fs. Only after 350 fs did we encounter noticeable deviations among the $\lambda_{\mathbf{P}} = 0.10$, 0.20, and 0.50 systems. Trajectories obtained under the electron injection conditions are similar only up to about 20 fs; deviations become noticeable after about 45 fs. Within the first 20 fs, the mean-field condition failed 5 times for the simulation with the criterion of $\lambda_{\mathbf{P}} = 0.05$, twice for $\lambda_{\mathbf{P}} = 0.10$, once for $\lambda_{\mathbf{P}} = 0.20$, and not at all for $\lambda_{\mathbf{P}} = 0.50$. By comparison, for the ground-state photoexcitation at the earliest times, mean-field dynamics is valid for 15−30 fs, while mean-field dynamics following electron injection is valid for 5−10 fs.

Nevertheless, the reason for MF failures is the same in both situations—coupling among electronic states. For electron injection, the frequency of MF projections and the observed rapid cascade through state space (see Figure 2) is due to the

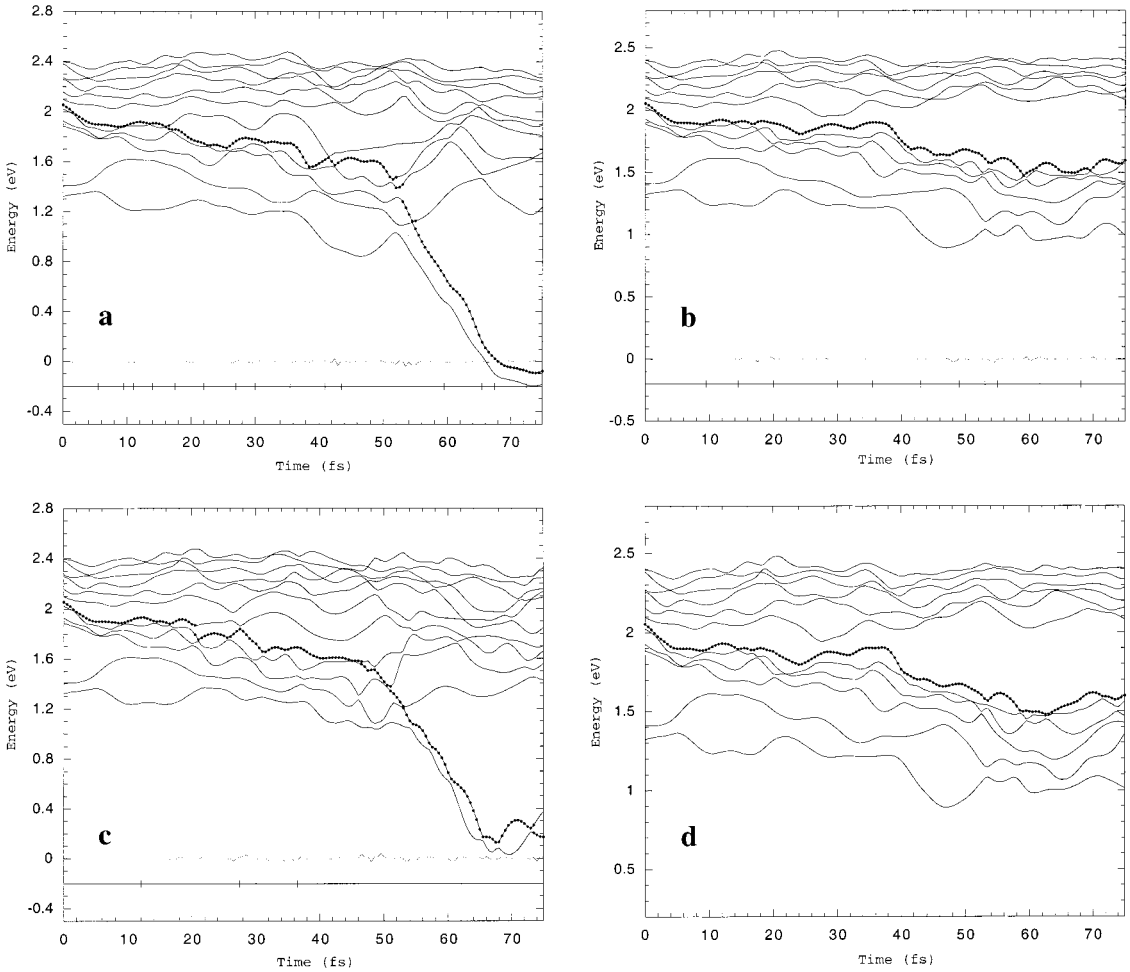

Figure 2. Short-time dynamical history of the adiabatic eigenstates for a typical set of trajectories following electron injection into pure water with mean-field momentum criterion $\lambda_{\mathbf{P}}$ set equal to (a) 0.05, (b) 0.10, (c) 0.20, and (d) 0.50. The bold trace shows the currently occupied state, while the vertical tick marks along the horizontal line at −0.20 eV indicate the times associated with a mean-field validity failure. The fluctuating line at 0 eV indicates deviations from energy conservation.

strong coupling among the poorly localized states of the injected electron. MF/SH determines a MF projection based on the deviation between the adiabatic and mean-field trajectories. As the auxiliary wave function develops into a superposition state, the mean-field force will eventually diverge from the reference Hellmann−Feynman force. In fact, the expression for the mean-field force[73] explicitly shows the importance of the NA coupling:

$$\mathbf{F}^{\mathrm{q}} = -\nabla_{\mathbf{R}}\langle\Psi(\mathbf{r};\mathbf{R})|H^{q}(\mathbf{r};\mathbf{R})|\Psi(\mathbf{r};\mathbf{R})\rangle$$

$$= -\sum_{\alpha}\sum_{k,j} c_k^{*} c_j[\langle\phi_k|\nabla_{\mathbf{R}_\alpha} H^{q}|\phi_j\rangle + \langle\nabla_{\mathbf{R}_\alpha}\phi_k|H^{q}|\phi_j\rangle + \langle\phi_k|H^{q}|\nabla_{\mathbf{R}_\alpha}\phi_j\rangle] \quad (27)$$

In an adiabatic basis, the quantum force on each classical particle α reduces to

$$\mathbf{F}_{\alpha}^{\mathrm{q}} = -\sum_{k}|c_k|^2[\nabla_{\mathbf{R}_\alpha}\epsilon_k(\mathbf{R})] - \sum_{k\neq j} c_k^{*} c_j[\epsilon_k(\boldsymbol{R}) - \epsilon_j(\mathbf{R})]\mathbf{d}_{kj}^{\alpha}(\mathbf{R}) \quad (28)$$

The first contribution to the mean-field force comes from the average of the forces evaluated from each adiabatic potential energy surface, weighted by the occupation of each state $|c_k|^2$. The second contribution in the direction of the NA coupling accounts for the effective force associated with mixing of surfaces.

As now anticipated, the state space trajectories deviate from each other as we vary the MF criterion due to differences in times of NA transition. Once the quantum subsystem changes state, the quantum force that drives the dynamics of the coupled quantum−classical system will be remarkably different from the other state forces. For the electron injection case, these transitions occur very early in time compared to the photoexcitation case. Figure 2a shows a series of NA transitions occurring in roughly the same time frame as the series shown in Figure 2c. The initial transition from the fifth to the fourth excited state perturbs the classical evolution. Subsequent mismatch between the transition times causes the trajectories to ultimately diverge from each other.

Determining how the MF projections contribute to the divergence is too complicated to ascertain. As noted earlier, small differences in trajectories can lead to NA transitions at different times with rapid divergence in the subsequent dynamics. This is illustrated in Figures 2 and 3. We first compare parts b and d of Figure 2 ($\lambda_{\mathbf{P}} = 0.10$ and 0.50). Both systems undergo a NA transition from the fifth to fourth excited state after about 75 fs following electron injection. During that time interval, the $\lambda_{\mathbf{P}} = 0.10$ environment has experienced 10 MF projections, while the $\lambda_{\mathbf{P}} = 0.50$ system has experienced three. The state space trajectories are similar up to 40 fs, with five projections for the more stringent criterion and a single projection for the relaxed one. In Figure 2c, with an intermediate $\lambda_{\mathbf{P}}$ value of 0.20, the choice of MF validity criterion affects the

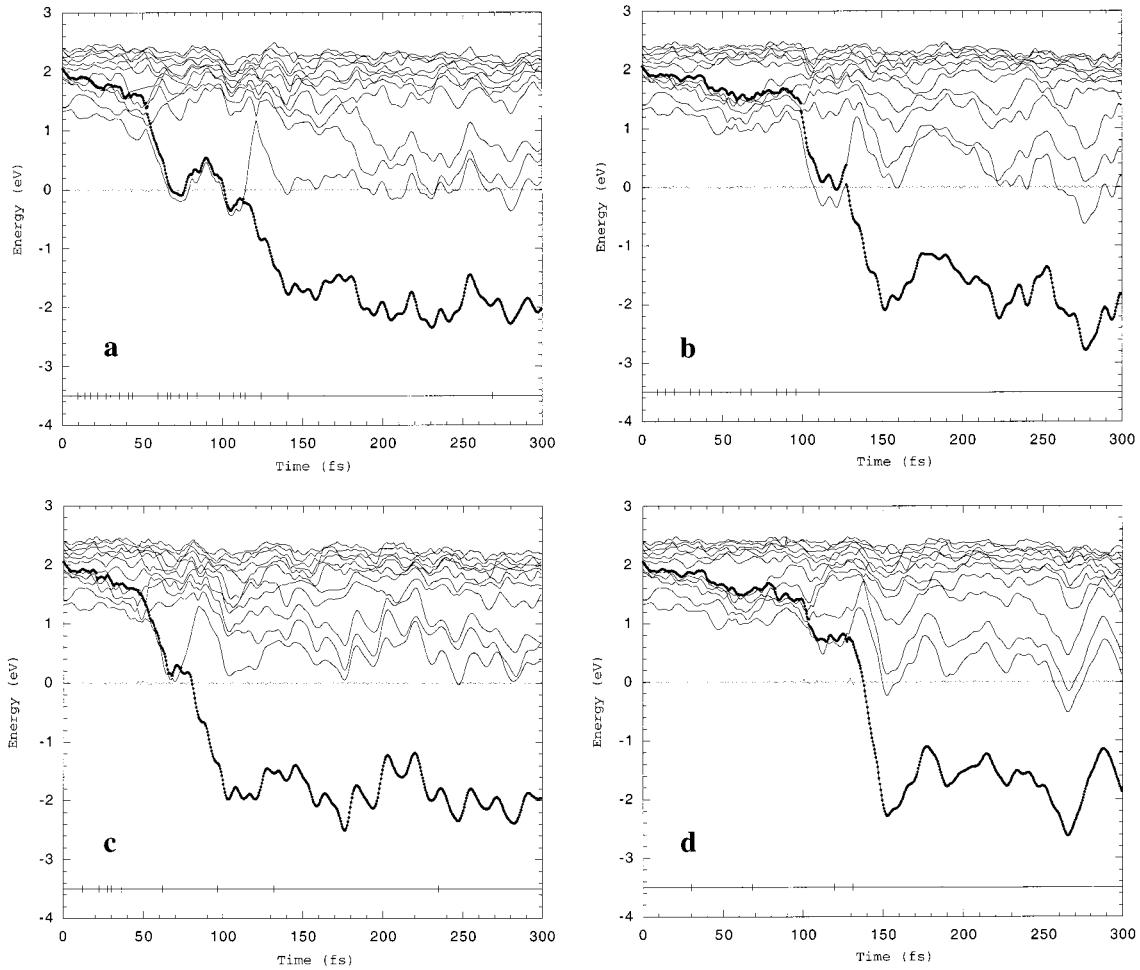

Figure 3. Dynamical history of the adiabatic eigenstates following electron injection into pure water. Trajectories are the same as those in Figure 2, but for longer time scales. The vertical ticks along the horizontal line at −4.5 eV indicate the times associated with a mean-field validity failure. The fluctuating line at 0 eV indicates deviations from energy conservation.

evolution of the primary wave function sufficiently that the single MF projection at 12 fs leads to a NA event 8 fs later. As stated previously, the interplay between the mean-field method and surface hopping prevents us from assigning a particular projection as more significant than others. One cannot determine a priori which criterion value gives the *important* projections at the appropriate time.

The important conclusion that one can draw is that for physically reasonable values of $\lambda_{\mathbf{P}} \sim 0.10-0.20$, MF projections occur only after a number of time steps (7−10 fs in this case), and that the dynamics is not a sensitive function of the MF criterion. Further, the time scale between MF projections is longer than the expected electronic coherence time.[33,34] (We note that the coherence time for the injection case has not been independently evaluated.) For the injection case, one might expect that the difference between MF/SH and MDQT trajectories is small at early times since the time between projections is small. However, the evidence that the adiabatic basis is a less accurate description of the states (i.e., manifestly strong mixing) tempers this expectation. Further studies along these lines of inquiry would be of interest.

Due to the simulation of dual trajectories, MF/SH is computationally more involved than MDQT. The 2-fold increase in computation cost stems from the additional (the reference trajectory) iterative solution of eigenvalues and eigenfunctions via the Lanczos algorithm. The quantum chemistry calculation is far more expensive than the classical dynamics used to generate the MF and reference trajectories. One could choose, when the system under study is computationally demanding, to implement an approximate MF/SH algorithm by propagating only the MF dynamics. An approximate reference trajectory is then generated by accumulating the reference Hellmann−Feynman forces along the MF trajectory. That is, step B in the algorithm above is discarded and the Hellmann−Feynman forces for the reference state k are evaluated from the eigenstate corresponding to the nuclear configurations comprising the MF trajectory. Our simulations of the hydrated electron show that this approximation is adequate for short times. The MF criteria are violated somewhat earlier in the full MF/SH algorithm than in this approximate scheme. However, given the range of criteria that appear acceptable, this does not present a limitation. Further, we note that simulations with a more stringent convergence criterion for the Lanczos algorithm[27,70] provided somewhat longer time scales for MF validity. Nevertheless, our choice of convergence criterion does enforce energy conservation, as evidenced by the horizontal line fluctuating about 0 eV in the figures. The accuracy of the results herein is adequate for verifying the viability of MF/SH for the simulation of large, realistic, strongly interacting systems.

Conclusion

To gain insight into the viability and behavior of the mean-field with surface hopping (MF/SH) algorithm for the simulation of complex chemical systems, we have implemented the method and performed nonadiabatic (NA) mixed quantum−classical

(MQC) molecular dynamics (MD) simulations for the aqueous solvated electron. Results reproduce key qualitative features observed in former simulations using stationary phase/surface hopping (SPSH).[27] The complexity of the SPSH algorithm in addition to the associated computational cost impeded the development of this method as a general purpose MQC MD scheme. The study reported here indicates MF/SH to be easily implementable and practical even for this experimentally accessible quantum−classical system. Although MF/SH is 2 times more computationally demanding than MDQT,[21] MF/SH is theoretically well founded at short times[11] and has the advantage that it more readily handles systems when the natural representation and the computational basis differ in the coupling region.[12] As such, we anticipate MF/SH to be useful for systems for which one does not have a priori knowledge of the adiabatic vs diabatic characteristics and for intermediate cases. An approximate form of the algorithm nearly eliminates the additional cost. The representative trajectories considered here delineate the important features of the MF/SH algorithm for the simulation of NA processes occurring in a prototype quantum−classical system. Mean-field dynamics proceed on a longer time scale in the first excited state environment than under the conditions of electron injection. The shorter time intervals between failure of the mean-field approximation in describing the relaxation dynamics following injection of an electron into water are due to the strong solvent-induced couplings among the delocalized states of the initial energetic electron. Trajectories associated with different choices of MF momentum criterion differ most notably in the time of NA events. They then quickly diverge from each other following a NA transition, as expected.

A primary motivation for the present work was the uncertainty as to whether the MF criteria would be violated so rapidly in a strongly coupled many-coordinate system that MF propagation for useful periods of time would not be possible, such that the MF/SH method would not be viable. The present results indicate first that the momentum criterion is the only one that needs to be considered. For the momentum criterion $\lambda_{\mathbf{p}}$ chosen in the anticipated physically reasonable range of 0.10−0.20, we do find that valid MF trajectories persist for many simulation steps. For the photoexcitation conditions, where the solvent is initially adapted to a somewhat similar electronic state, the MF propagation remains valid for 30−70 fs, equal to a comparable number of solvent time steps and many times the electronic coherence time scale. For electron injection conditions, the times are shorter, 7−10 fs, but retain the same viability of the algorithm. It is also worth noting that these results may provide some useful guidelines for applicability of a pure MF propagation.

For systems exhibiting extensive solute−solvent coupling involving many bath modes, such as the aqueous solvated electron, the details with which we treat the loss of coherence[76] among diverging alternative nuclear paths can dramatically influence the NA transition probabilities.[33] To be valid, the characteristic time between successive collapses of the system superposition state unto a pure state due to MF failures or surface hops should be considerably greater than this coherence time. As can be seen from eq 18, the stochastic procedure used for determining a NA transition is directly related to the coherence, p_{kj}. Maintaining coherence for a longer time interval facilitates the probability of a transition whereas a collapse of the wave function unto a pure state limits the transition probability. The present work indicates that artificial decoherence introduced by the MF/SH algorithm will occur on a considerably longer time scale than the underlying physical decoherence.[33,34]

Decoherence can be easily introduced in MF/SH by employing a reduction mapping technique[74,75] or by a direct damping of the nondiagonal density matrix elements as suggested by Tully.[14] Work is currently in progress to study the behavior of the solvated electron as a function of the decoherence time scales using a decoherent version of the MF/SH algorithm. The inclusion of decoherence in MF/SH will be the topic of future studies of the solvated electron in water and in methanol.

Acknowledgment. This work was supported by a grant from the National Science Foundation. K.F.W. thanks Dr. Daren M. Lockwood for his stimulating questions and helpful discussions.

References and Notes

(1) *Classical and Quantum Dynamics in Condensed Matter Simulations*; Berne, B. J., Ciccotti, G., Coker, D. F., Eds.; World Scientific: New Jersey, 1998.
(2) *Modern Methods for Multidimensional Dynamics Computations in Chemistry*; Thompson, D. L., Ed.; World Scientific: New Jersey, 1998.
(3) Ehrenfest, P. *Z. Phys.* **1927**, *45*, 455.
(4) Mittelman, M. H. *Phys. Rev.* **1961**, *122*, 449.
(5) Mott, N. F. *Proc. Cambridge Philos. Soc.* **1931**, *27*, 553.
(6) Dirac, P. A. M. *Proc. Cambridge Philos. Soc.* **1930**, *26*, 376.
(7) Heller, E. J. *J. Chem. Phys.* **1976**, *64*, 63.
(8) Delos, J. B.; Thorson, W. R.; Knudson, S. K. *Phys. Rev. A* **1972**, *6*, 709.
(9) Delos, J. B.; Thorson, W. R. *Phys. Rev. A* **1972**, *6*, 720.
(10) Kuntz, P. J. *J. Chem. Phys.* **1991**, *95*, 141.
(11) Tully, J. C. In *Classical and Quantum Dynamics in Condensed Phase Simulations*; Berne, B. J., Ciccotti, G., Coker, D. F., Eds.; World Scientific: Singapore, 1998.
(12) Prezhdo, O. V.; Rossky, P. J. *J. Chem. Phys.* **1997**, *107*, 825.
(13) Tully, J. C.; Preston, R. K. *J. Chem. Phys.* **1971**, *55*, 562.
(14) Tully, J. C. *J. Chem. Phys.* **1990**, *93*, 1061.
(15) Smith, B. R.; Bearpark, M. J.; Robb, M. A.; Bernardi, F.; Olivucci, M. *Chem. Phys. Lett.* **1995**, *242*, 27.
(16) Parlant, G.; Gislason, E. A. *J. Chem. Phys.* **1989**, *91*, 4416.
(17) Gersonde, I. H.; Gabriel, H. *J. Chem. Phys.* **1993**, *98*, 2094.
(18) Stine, J. R.; Muckerman, J. T. *J. Chem. Phys.* **1976**, *65*, 3975.
(19) Blais, N. C.; Truhlar, D. G. *J. Chem. Phys.* **1983**, *79*, 1334.
(20) Jones, K. R. W. *Phys. Rev. Lett.* **1996**, *76*, 4087.
(21) Hammes-Schiffer, S.; Tully, J. C. *J. Chem. Phys.* **1994**, *101*, 4657.
(22) Chapman, S. *Adv. Chem. Phys.* **1992**, *82*, 423.
(23) Kapral, R.; Ciccotti, G. *J. Chem. Phys.* **1999**, *110*, 8919.
(24) Wan, C.-C.; Schofield, J. *J. Chem. Phys.* **2000**, *112*, 4447.
(25) Nielsen, S.; Kapral, R. *J. Chem. Phys.* **2000**, *112*, 6543.
(26) Volobuev, Y. L.; Hack, M. D.; Topaler, M. S.; Truhlar, D. G. *J. Chem. Phys.* **2000**, *112*, 9716.
(27) Webster, F.; Rossky, P. J.; Friesner, R. A. *Comput. Phys. Commun.* **1991**, *63*, 494.
(28) Pechukas, P. *Phys. Rev.* **1969**, 181, 174.
(29) Webster, F.; Wang, E. T.; Rossky, P. R.; Friesner, R. A. *J. Chem. Phys.* **1994**, *100*, 4835.
(30) Schwartz, B. J.; Rossky, P. J. *J. Phys. Chem.* **1994**, *98*, 4489.
(31) Schwartz, B. J.; Rossky, P. J. *J. Chem. Phys.* **1994**, *101*, 6902.
(32) Schwartz, B. J.; Rossky, P. J. *J. Chem. Phys.* **1994**, *101*, 6917.
(33) Prezhdo, O. V.; Rossky, P. J. *J. Chem. Phys.* **1997**, *107*, 5863.
(34) Schwartz, B. J.; Bittner, E. R.; Prezhdo, O. V.; Rossky, P. J. *J. Chem. Phys.* **1996**, *104*, 5942.
(35) Sheu, W.-S.; Rossky, P. J. *J. Phys. Chem.* **1996**, *100*, 1295.
(36) Decornez, H.; Drukker, K.; Hurley, M. M.; Hammes-Schiffer, S. *Ber. Bunsen. Ges. Phys. Chem.* **1998**, *102*, 533.
(37) Drukker, K.; de Leeuw, S. W.; Hammes-Schiffer, S. *J. Chem. Phys.* **1998**, *108*, 6799.
(38) Hammes-Schiffer, S. In *Advances in Classical Trajectory Methods*, Vol. 3; Hase, W. S., Ed.; JAI Press: London, 1998.
(39) Space, B.; Coker, D. F. *J. Chem. Phys.* **1991**, *94*, 1976.
(40) Space, B.; Coker, D. F. *J. Chem. Phys.* **1992**, *96*, 652.
(41) Ferretti, A.; Granucci, G.; Lami, A.; Persico, M.; Villani, G. *J. Chem. Phys.* **1996**, *104*, 5517.
(42) Ito, M.; Ohmine, I. *J. Chem. Phys.* **1997**, *106*, 3159.
(43) Vachev, V. D.; Frederick, J. H.; Grishanin, B. A.; Zadkov, V. A.; Koroteev, N. I. *J. Phys. Chem.* **1995**, *99*, 5247.
(44) Krylov, A. I.; Gerber, R. B.; Coalson, R. D. *J. Chem. Phys.* **1996**, 105, 4626.
(45) Staib, A.; Borgis, D. *J. Chem. Phys.* **1995**, *103*, 2642.
(46) Lobaugh, J.; Rossky, P. J. *J. Phys. Chem. A* **1999**, *103*, 9432.
(47) Alfano, J. C.; Walhout, P. K.; Kimura, Y.; Barbara, P. F. *J. Chem. Phys.* **1993**, *98*, 5996.

(48) Kimura, Y.; Alfano, J. C.; Walhout, P. K.; Barbara, P. F. *J. Phys. Chem.* **1994**, *98*, 3450.
(49) Walhout, P. K.; Alfano, J. C.; Kimura, Y.; Silva, C.; Reid, P. J.; Barbara, P. F. *Chem. Phys. Lett.* **1995**, *232*, 135.
(50) Reid, P. J.; Silva, C.; Walhout, P. K.; Barbara, P. F. *Chem. Phys. Lett.* **1994**, *228*, 658.
(51) Silva, C.; Walhout, P. K.; Yokoyama, K.; Barbara, P. F. *Phys. Rev. Lett.* **1998**, *80*, 1086.
(52) Shi, X.; Long, F. H.; Lu, H.; Eisenthal, K. B. *J. Phys. Chem.* **1995**, *99*, 6917.
(53) Shi, X.; Long, F. H.; Lu, H.; Eisenthal, K. B. *J. Phys. Chem.* **1996**, *100*, 11903.
(54) Gauduel, Y.; Pommeret, S.; Yamada, N.; Migus, A.; Antonetti, A. In *Ultrafast Phenomena VII*; Harris, C. B., Ippen, E. P., Mourou, G. A., Zewail, A. H., Eds.; Springer-Verlag: New York, 1990.
(55) Long, F. H.; Lu, H.; Eisenthal, K. B. *Phys. Rev. Lett.* **1990**, *64*, 1469.
(56) Long, F. H.; Lu, H.; Shi, X.; Eisenthal, K. B. *Chem. Phys. Lett.* **1990**, *169*, 165.
(57) Long, F. H.; Shi, X.; Lu, H.; Eisenthal, K. B. *J. Phys. Chem.* **1994**, *98*, 7252.
(58) Tully, J. C. In *Modern Theoretical Chemistry: Dynamics of Molecular Collisions*; Miller, W. H., Ed.; Plenum: New York, 1976.
(59) Epstein, S. T. In *Force Concept in Chemistry*; Deb, B. M., Ed.; Van Nostrand Reinhold: New York, 1981.
(60) Dunne, L. J.; Murrell, J. N.; Stamper, J. G. *Chem. Phys. Lett.* **1984**, *112*, 497.
(61) Coker, D. F.; Xiao, L. *J. Chem. Phys.* **1995**, *102*, 496.
(62) Müller, U.; Stock, G. *J. Chem. Phys.* **1997**, *107*, 6230.
(63) Coker, D. F. In *Computer Simulations in Chemical Physics*; Allen, M. P., Tildesley, D. J., Eds.; Kluwer Academic: Netherlands, 1993.
(64) Tully, J. C. *Int. J. Quantum Chem. Quantum Chem. Symp.* **1991**, *25*, 299.
(65) Herman, M. F. *J. Chem. Phys.* **1984**, *81*, 754.
(66) Toukan, K.; Rahman, A. *Phys. Rev. B* **1985**, *31*, 2643.
(67) Murphrey, T. H.; Rossky, P. J. *J. Chem. Phys.* **1993**, *99*, 515.
(68) Allen, M. P.; Tildesley, D. J. *Computer Simulation of Liquids*; Clarendon: Oxford, 1987.
(69) Schnitker, J.; Rossky, P. J. *J. Chem. Phys.* **1987**, *86*, 3462.
(70) Cullum, J. K.; Willoughby, R. A. *Lanczos Algorithms for Large Symmetric Eigenvalue Computations Vol. 1 Theory*; Birkhäuser: Boston, 1985.
(71) Press, W. H.; Teukolsky, S. A.; Vetterling, W. T.; Flannery, B. P. *Numerical Recipes in Fortran 77*; Cambridge University: Cambridge, 1992.
(72) Webster, F. J.; Schnitker, J.; Friedrichs, M. S.; Friesner, R. A.; Rossky, P. J. *Phys. Rev. Lett.* **1991**, *66*, 3172.
(73) Tully, J. C. In *Modern Methods for Multidimensional Dynamics Computations in Chemistry*, Thompson, D. L., Ed.; World Scientific: New Jersey, 1998.
(74) Bittner, E. R.; Rossky, P. J. *J. Chem. Phys.* **1995**, *103*, 8130.
(75) Bittner, E. R.; Rossky, P. J. *J. Chem. Phys.* **1997**, *107*, 8611.
(76) Onuchic, J. N.; Wolynes, P. G. *J. Phys. Chem.* **1988**, *92*, 6495.